



Trans. Nonferrous Met. Soc. China 33(2023) 3812–3824

Transactions of Nonferrous Metals Society of China

www.tnmsc.cn



Selective depressing mechanism of H-acid monosodium salt on flotation separation of graphite and sphalerite

Yong ZENG^{1,2}, Cui WANG^{1,2}, Jian-feng HE^{1,2}, Zhong-bao HUA^{1,2}, Kai CHENG^{1,2}, Xi-qing WU^{1,2}, Wei SUN^{1,2}, Li WANG^{1,2}, Jia-cheng HU³, Hong-hu TANG^{1,2}

School of Minerals Processing and Bioengineering, Central South University, Changsha 410083, China;
Key Laboratory of Hunan Province for Clean and Efficient Utilization of
Strategic Calcium-containing Mineral Resources, Central South University, Changsha 410083, China;
State Key Laboratory of Multiphase Complex Systems, Institute of Process Engineering,

Chinese Academy of Sciences, Beijing 100190, China Received 13 July 2022; accepted 6 December 2022

Abstract: Micro-flotation experiments, Fourier transform infrared spectroscopy (FT-IR) tests, Zeta potential tests, X-ray photoelectron spectroscopy (XPS) analysis and molecular dynamics simulation were used to study the flotation behavior, separation and depressing mechanisms of graphite and sphalerite in the presence of H-acid monosodium salt (HAMS). Under the optimum flotation conditions, the recovery of sphalerite and graphite in the concentrate of mixed mineral flotation was 93.37% and 4.98%, respectively. Zeta potential tests and XPS analysis indicated that HAMS was considerably adsorbed on graphite surfaces but virtually absent on sphalerite surfaces. The FT-IR tests revealed that HAMS had no significant chemisorption on graphite surfaces. Molecular dynamics simulation inferred that the hydrophobic interaction between the naphthalene ring in HAMS and graphite was responsible for the adsorption of HAMS on the graphite surface.

Key words: H-acid monosodium salt; graphite; sphalerite; flotation separation; molecular dynamics simulation

1 Introduction

Sphalerite is the primary raw material for zinc metal, and it is frequently found in deposits alongside graphite. Sulfide deposits containing graphite have been discovered all over the world, including the Century Mine at Lawn Hill in Australia, the Langshan–Zhaeriaishan district in China, and the Aravalli–Delhi orogenic belt in India [1–3]. According to reports, the graphite content of Jiashenpan lead–zinc ore in China was 2.61%, while that of Rampura–Agucha lead–zinc ore in India was 12% [4,5]. Graphite is a crystalline mineral of carbon with a distinctive layered structure [6]. The electric neutrality of the surface

contributes to its high hydrophobicity [7]. The natural hydrophobicity of graphite makes its enrichment in the froth product of sulfide ore flotation inevitable. Graphite may also be easily smeared on the surface of hydrophilic gangue minerals to improve their floatability [5]. These degrade the grade of the final sphalerite concentrate and make future smelting more challenging [8]. Graphite pre-flotation is frequently used to remove graphite and coated hydrophilic minerals in sphalerite cleaning. However, there were drawbacks to this approach, including the loss of valuable metals, excessive reagent consumption, and limited carbon recovery [5,8]. Another strategy is to add depressants to the roughing process to prevent graphite from entering the subsequent cleaning.

The strategy described above was conducted under the circumstance that graphite and sphalerite monomers dissociate. However, graphite and sphalerite coexist in proximity [5]. To avoid sphalerite loss due to excessive comminution, the undissociated graphite and sphalerite must be floated together in the roughing, depressed in the cleaning, and finally dissociated in the mill, according to our technique. As a result, the depressant's effectiveness is crucial in the rejection of graphite from sulfide ore flotation. The main graphite selectivity depressants reported in the literature are dextrin and its modifiers, starch and its modifiers, bagasse, carboxymethyl cellulose (CMC), synthetic dyes, humic lignosulphonates [5,7–14].

There are many reports of dextrin as a graphite depressant in experimental and theoretical research. BEAUSSART et al [9] studied the adsorption of phenyl succinate dextrin and styrene oxide dextrin (two types of modified dextrin) on graphite and sphalerite. The results showed that they could sharply deteriorate the hydrophobicity of graphite surfaces, while the hydrophobicity of sphalerite surfaces would only decrease significantly after being treated with styrene oxide dextrin. Dextrin has already been proven to have the ability to adsorb on mineral surface via metal hydroxy species [15-18]. SUBRAMMIAN et al [19] found that the presence of metal ions on the surface of graphite was the main reason for dextrin adsorption, and the adsorption density was strongly correlated with the number of metal sites on the graphite surfaces. A molecular dynamics simulation was used to study the adsorption process of dextrin on graphite surface, and the conclusion of hydrophobichydrophobic interaction between graphite and dextrin was obtained [20]. SOLONGO [14] reported that the electrolyte enhanced the adsorption of CMC on the graphite surface. Adsorption can be nearly be ignored in the absence of an electrolyte. The cation activation sites of the graphite surface generated from electrolyte addition were connected to CMC by electrostatic interaction. CHIMONYO [8] investigated the depression of native wheat starch and an oxidized starch derivative on graphite and chalcopyrite. The oxidized starch derivative shows good selective adsorption performance on the surfaces of the two minerals and has high separation efficiency in flotation.

However, polysaccharide depressants graphite usually cause the instability problem of foam performance in practice and they are not atom economic since most of the reagent molecular are inactive. Therefore, it is essential to find a novel small molecule depressant of graphite. In this study, we first investigated the application of a small organic molecule depressant called monosodium salt to depress graphite in sulfide ore. experiments, FT-IR analysis, Flotation potential tests, XPS analysis, and molecular dynamics simulation were used to investigate the behavior and mechanism of flotation separation of graphite and sphalerite.

2 Experimental

2.1 Materials and reagents

The natural flake graphite used in this study was obtained from Laixi City, Shandong Province, a famous graphite ore producing area in China. The XRD pattern is shown in Fig. 1(a). Sphalerite was obtained from Guangdong Province, China. Its XRD pattern is shown in Fig. 1(b). After manual

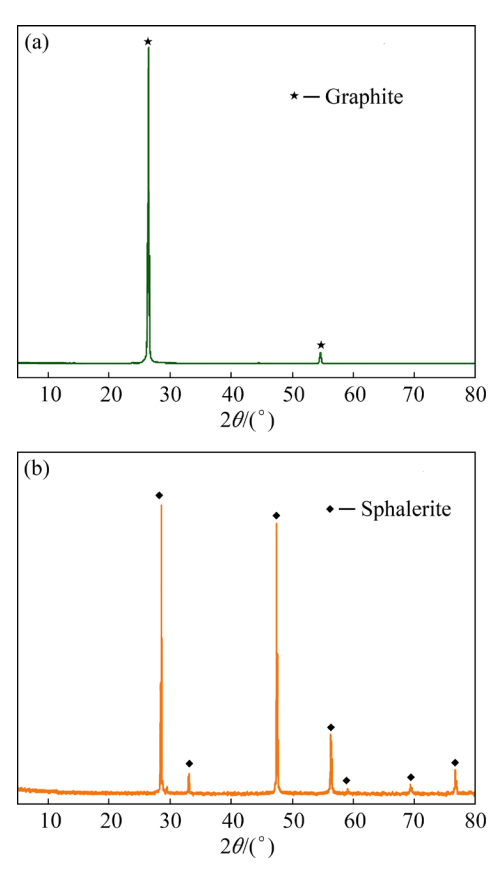


Fig. 1 XRD patterns of graphite (a) and sphalerite (b)

crushing, sphalerite was ground by a ceramic tumbling ball mill and sieved to obtain grain size of 38 to 76 μ m for flotation and tests. Graphite was sieved after mechanical crushing to obtain the grain size of 38 to 180 μ m for flotation and tests. Deionized water was used for all tests and flotation.

The molecular structure of HAMS, one of the most common organic chemical compounds of naphthalenesulfonic acid, is depicted in Fig. 2. Because of its simple molecular structure, it was employed as a dye and medicine production intermediate [21,22]. HAMS and methyl isobutyl carbinol (MIBC) were purchased from Shanghai Macklin Biochemical Co., Ltd., and their purity is over 80% and 98%, respectively. The collector is industry-grade sodium butyl xanthate (SBX). Analytical-grade activator CuSO₄·5H₂O, regulator HCl and NaOH were purchased from Sinopharm Chemical Reagent Co., Ltd.

Fig. 2 Molecular structure of HAMS

2.2 Micro-flotation experiments

The micro-flotation tests were conducted on an XFD flotation machine. 2 g of mineral samples (for the mixed mineral of sphalerite and graphite micro-flotation test, the mass ratio of sphalerite to graphite was 1:1) were weighed and dispersed in a plexiglass flotation cell filled with 35 mL of deionization water. The stirring rate of the flotation machine was controlled at 1650 r/min. It was stirred for 3 min before adding the reagent to ensure that the solution was adequately mixed with the mineral sample. The activator, depressant, collector and frother were added to the mixed solution in sequence and stirred for 3, 3, 3 and 1 min. The pH value was adjusted to the set value in the whole process of reagent addition. The flotation time was 6 min. After flotation, the concentrate product in the foam and the tailing product in the cell were filtered, dried, and weighed, respectively.

2.3 FT-IR spectroscopy tests

The Shimadzu IR Affinity-1 Fourier Infrared Spectrometer was used for testing, and the wavenumber range was 4000–400 cm⁻¹. The graphite and sphalerite were ground to less than 5 µm in an agate mortar. The flotation machine was used as a stirrer to deal with the interaction of minerals and reagents. The addition sequence of reagent was consistent with that of flotation, and the treatment time was 2 h. After the treatment of the flotation machine, the pulp was filtered and washed with deionized water for two times. Finally, it was dried at 35 °C in a vacuum drying oven and used for infrared testing.

2.4 Zeta potential tests

Samples used for the Zeta potential test were ground with agate mortar to a particle size of less than 5 µm. 5 mg of samples that were ground mixed with 100 mL of deionized water, and stirred with a magnetic stirrer continuously. Activator and depressant were inserted after pH adjustment with NaOH. The treatment time of the reagent on the mineral surface was completely consistent with flotation, and standing for 5 min after stirring. Finally, the supernatant was extracted and injected into the electrophoresis cell. Measuring the ζ potential in micro electrophoresis instrument of Malvern Nano ZS 90. Each measurement was replicated three times and the average value was obtained. In a potassium nitrate solution with a concentration of 1×10⁻³ mol/L, the entire Zeta potential test was carried out. All of the tests had a pH of (10±0.05) in them.

2.5 X-ray photoelectron spectroscopy (XPS) tests

XPS measurement was performed by ESCALAB 250Xi of ThermoFisher-VG Scientific Company of the United States. A 2 g of ore sample was added to the flotation cell before the addition of reagents. After adjusting the pH according to the flotation test process, metal ions and depressants were added. The treatment time of reagent on the mineral surface was completely consistent with flotation. Finally, the sample in the cell was filtered and drying it in the vacuum drying oven at 35 °C.

2.6 Molecular dynamics simulation model and method

The whole process, including model

establishment, geometry optimization, and molecular dynamics simulation, was completed in Materials Studio 2017 software (Accelrys, USA). The DMol3 module was used to optimize the geometry of HAMS. 2000 water molecules and 5 HAMS molecules were placed on the surface of graphite by Packing function in the Amorphous Cell module to simulate the aqueous environment of flotation, and 5 sodium ions were used for charge balance. A vacuum layer of 120 Å was constructed along the z-axis to eliminate the periodic boundary. The Forcite module was used for molecular dynamics simulation of the reagentwater-graphite mixture model. The forcefield of Condensed-phase optimized molecular potentials for atomistic simulation studies (COMPASS) was adopted for all simulations. The 1 ns total simulation time and 1 fs simulation time step were performed in molecular dynamics simulation, which was carried out in a 298 K constant-particle number, -volume and -temperature (NVT) ensemble using a Nose thermostat. The electrostatic and Van der Waals interactions were calculated using Ewald summation method, and the Ewald accuracy was 0.42 J/mol.

3 Results and discussion

3.1 Micro-flotation experiments

3.1.1 Single mineral flotation

The effects of HAMS concentration and pH value on the flotation behavior of sphalerite and graphite were examined by single mineral flotation, respectively (Fig. 3). As shown in Fig. 3(a), the flotation recoveries of both sphalerite and graphite were more than 95% in the absence of HAMS. For sphalerite, the increase in HAMS dosage from 5.0×10^{-4} to 4.0×10^{-3} mol/L only has a negligible effect on its flotation recovery. Even if the HAMS dosage was increased to 6.0×10^{-3} mol/L, the flotation recovery of sphalerite remains above 90%. For graphite, its flotation recovery was very sensitive to HAMS dosage. When the dosage of HAMS increases to 1.0×10⁻³ mol/L, the recovery of graphite flotation decreases sharply to about 40.97%. Then, the downward trend of flotation recovery goes to be flat with the increase of HAMS dosage from 1.0×10^{-3} to 4.0×10^{-3} mol/L, achieving an equilibrium between 5.0×10⁻³ and 6.0×10^{-3} mol/L. The obvious phenomenon was that the flotation recovery difference between graphite and sphalerite reached its maximum when the HAMS dosage was 5.0×10^{-3} mol/L.

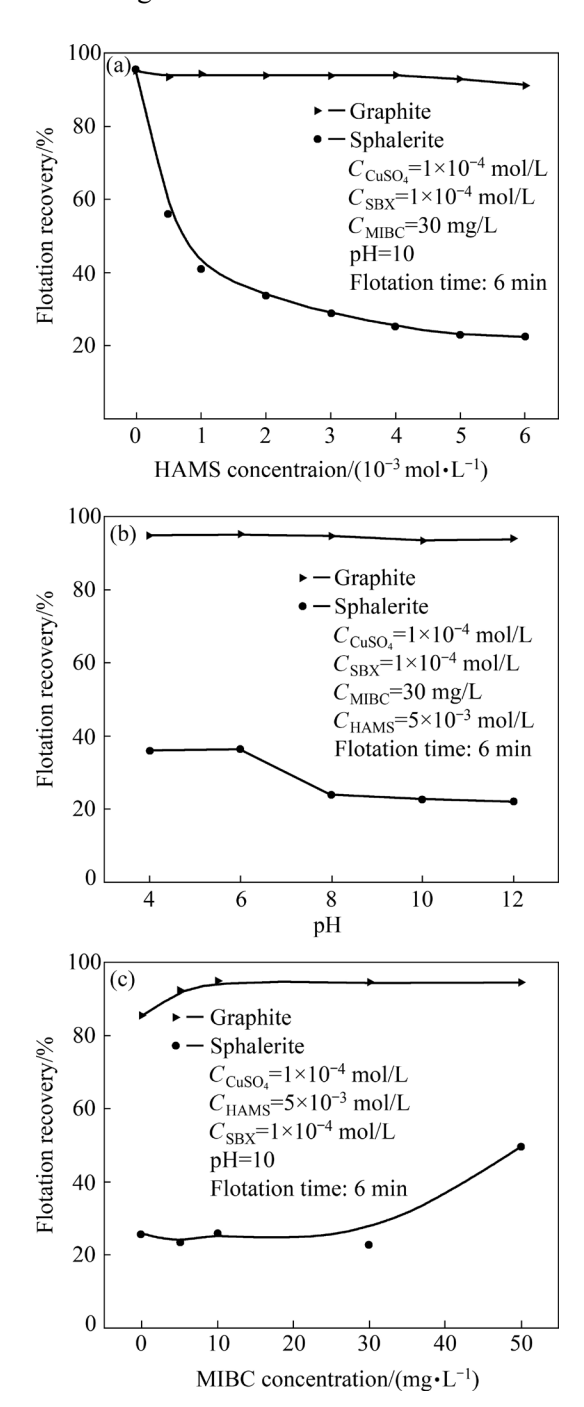


Fig. 3 Effect of HAMS concentration (a), pH (b), and MIBC concentration (c) on sphalerite and graphite flotation recovery

Figure 3(b) shows the effect of pH on flotation recoveries of sphalerite and graphite at a SBX concentration of 1×10^{-4} mol/L and a HAMS concentration of 5.0×10^{-3} mol/L. The result illustrates that the recovery of sphalerite was nearly free from the difference in pH. For graphite, the

flotation recovery was more than 35% in acidic condition, and less than 30% in the alkaline condition.

The dosage of MIBC (Frother) for single mineral flotation was also investigated, and the results are presented in Fig. 3(c). The sphalerite and graphite recovery increased with the increase in MIBC dosage. When the MIBC concentration was 10 mg/L, the recovery of sphalerite was 94.76% and the recovery of graphite was 25.82%. Further increasing the dosage of MIBC would have no effect on sphalerite recovery. However, the flotation recovery of graphite would significantly increase when the MIBC dosage increased to 50 mg/L. This result inferred that the entrainment of the foam had a great effect on the floatation of graphite, which would weaken the selective flotation separation of graphite and sphalerite.

3.1.2 Mixed mineral flotation

The effects of HAMS dosage, SBX dosage, MIBC dosage and flotation time on the flotation behavior of sphalerite and graphite (1:1) mixed

samples were investigated using mixed mineral flotation (Fig. 4). As shown in Fig. 4(a), the addition of HAMS has negligible effects on the recovery of sphalerite. Even if the HAMS dosage increased to more than 4.0×10^{-3} mol/L, its recovery was still more than 93%. However, graphite shows a sharp sensitivity to HAMS. The flotation recovery of graphite decreased from 95.02% to 21.27% with the increase of HAMS from 0 to 2.0×10^{-3} mol/L.

Considering the influence of flotation foam entrainment on graphite recovery, the dosage of SBX, MIBC, and flotation time were studied due to their effects on the foams. As shown in Fig. 4(b), the flotation performance of sphalerite and graphite is not satisfactory in the absence of SBX. When the SBX dosage increased from 0 to 0.5×10^{-4} mol/L, the recovery of sphalerite increased from 2.64% to 92.61%, while the recovery of graphite increased from 9.6% to 12.02%. Further enhancing the dosage of SBX did not significantly improve the recovery of sphalerite but sharply increased the recovery of graphite.

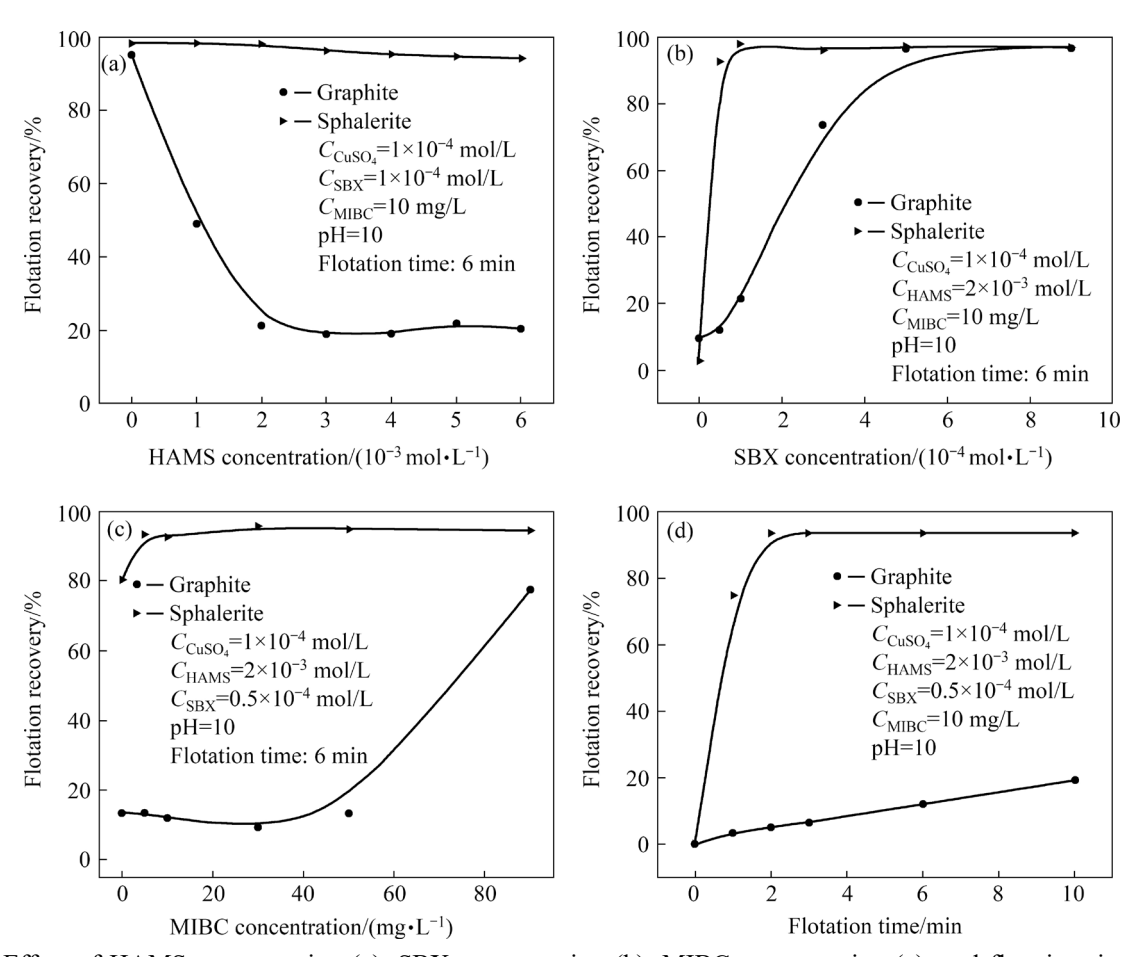


Fig. 4 Effect of HAMS concentration (a), SBX concentration (b), MIBC concentration (c), and flotation time (d) on flotation recovery of mixed minerals

As displayed in Fig. 4(c), when the MIBC dosage was 0, the sphalerite recovery was 80.32% and the graphite recovery was 13.46%. With the dosage of MIBC increased to 10 mg/L, the recovery of sphalerite increased to 92.61%, and the recovery of graphite did not change significantly. Further increasing the dosage of MIBC has little effect on sphalerite recovery but greatly improves graphite recovery.

As shown in Fig. 4(d), the recovery of sphalerite rapidly increased to more than 90% within the first 2 min and stayed almost the same in the following 4 min. However, the graphite recovery showed a stable linear increasing rate of 2% per minute, and a suitable flotation time for separation would be 2 min. The optimum flotation performance was obtained at 1.0×10^{-4} mol/L CuSO₄, 2.0×10^{-3} mol/L HAMS, 5.0×10^{-5} mol/L SBX, 10 mg/L MIBC and flotation for 2 min, and the recovery of sphalerite and graphite was 93.37% and 4.98%, respectively.

3.2 FT-IR analysis

FT-IR analysis is a powerful tool for studying reagent adsorption on mineral surfaces. The infrared spectra of graphite and sphalerite before and after reagent treatment are shown in Figs. 5(a) and (b), respectively. As shown in Fig. 5(a), the treatment of HAMS and SBX did not result in the addition of new stretching vibration absorption to the graphite spectra, indicating that they were not adsorbed on the graphite surface via chemical and electrostatic adsorption. It was consistent with the electrically neutral graphite surface's nature.

As shown in Fig. 5(b), there is no discernible

change in the infrared spectra of sphalerite after HAMS treatment, which is analogous to graphite. SBX treatment, on the other hand, resulted in a stretching vibration peak of -Cu-SBX and dixanthogen. They were located at 1037.52 and 1197.58 cm⁻¹, respectively [23,24]. HAMS has no noticeable chemical or electrostatic adsorption on the surface of sphalerite, whereas SBX was stridently adsorbed on the surface of sphalerite due to chemical bonding.

3.3 Zeta potential analysis

The surface potential of graphite and sphalerite at different HAMS concentrations is shown in Fig. 6(a). Cu ions were added to all potential tests to be compatible with the flotation experiments. When only CuSO₄ was added to the sample aqueous solution (i.e. the HAMS concentration was 0 mol/L), the surface potential on graphite was -13.9 mV and -10.84 mV on sphalerite. The graphite surface lost potential rapidly with the addition of HAMS. However, the surface potential of sphalerite was different from that of graphite. It decreased slowly with an increase in HAMS concentration. The surface potential of graphite decreased to -48.23 mV with the increase in HAMS concentration to 1×10⁻⁴ mol/L, and sphalerite decreased to -10.84 mV. With the increase of HAMS concentration, the surface potential of graphite finally decreased by 43.10 mV, while that of sphalerite decreased by 23.40 mV. The above results indicated that HAMS was more easily adsorbed on the graphite surface.

To understand the potential changes caused by SBX on HAMS-treated mineral surfaces, the

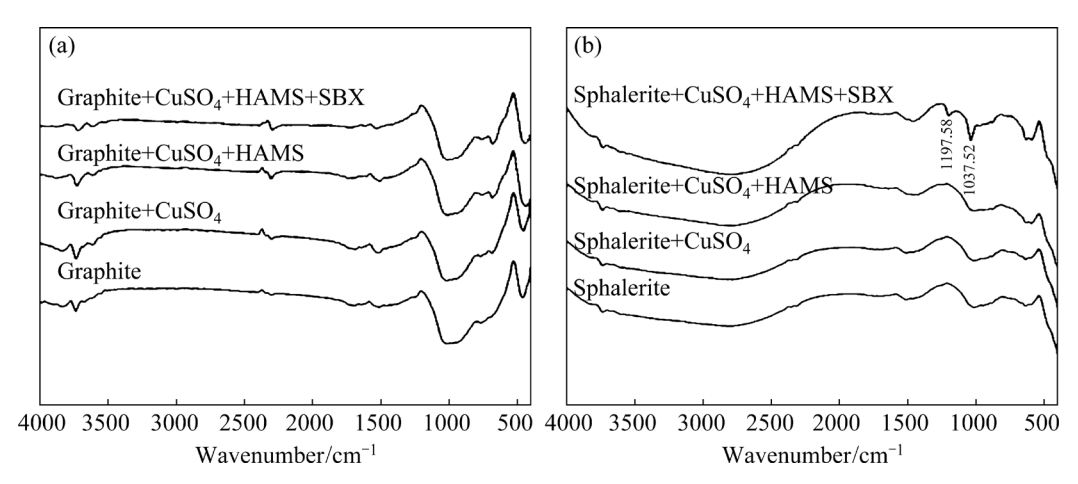


Fig. 5 FT-IR spectra of graphite (a) and sphalerite (b)

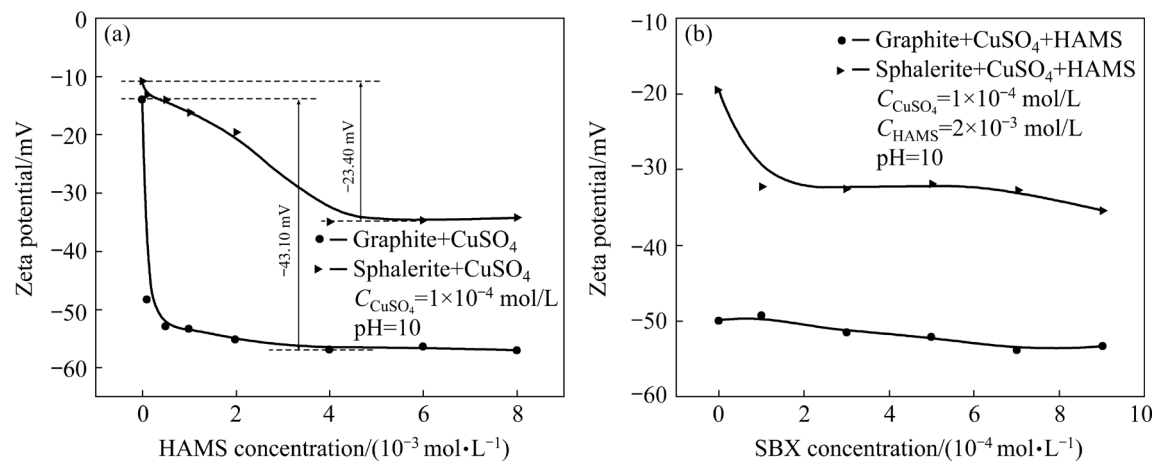


Fig. 6 Effect of HAMS concentration (a) and SBX concentration (b) on Zeta potential of graphite and sphalerite

surface potential of HAMS-treated graphite and HAMS-treated sphalerite in the different SBX concentrations is shown in Fig. 6(b). As presented in Fig. 6(b), the Zeta potentials of graphite and sphalerite decreased with an increase in SBX concentration. The surface potential of sphalerite decreased significantly after addition of SBX. However, the surface potential of graphite decreased slightly after adding SBX. It was indicated that the adsorption density of SBX on sphalerite was greater compared with graphite after HAMS treatment.

3.4 XPS analysis

XPS was frequently employed to identify the mechanism of interaction between chemical reagents and mineral surfaces during flotation [25–28]. Therefore, the XPS measurement was performed to further exploring the separation mechanism of HAMS on graphite and sphalerite. 3.4.1 O 1s

Figure 7 depicts the HAMS O 1s spectra. Table 1 summarizes its peak fitting parameters and O 1 assignment. As displayed in Fig. 7 and Table 1, the peaks at 531.50 eV and 533.21 eV were attributed to O—S and —OS, respectively [29,30].

Figure 8 presents the O 1s spectra of graphite and sphalerite in the absence and presence of HAMS. The peak fitting parameters and assignment of O 1s were summarized in Table 1. As displayed in Fig. 8(a) and Table 1, the peaks at 531.28 eV (531.14 eV), 532.45 eV (532.32 eV) and 533.73 eV (533.67 eV) were attributed to surface hydroxyl (—OH), —COO⁻ and H₂O, respectively. They may come from oxidizing impurities and adsorbed water

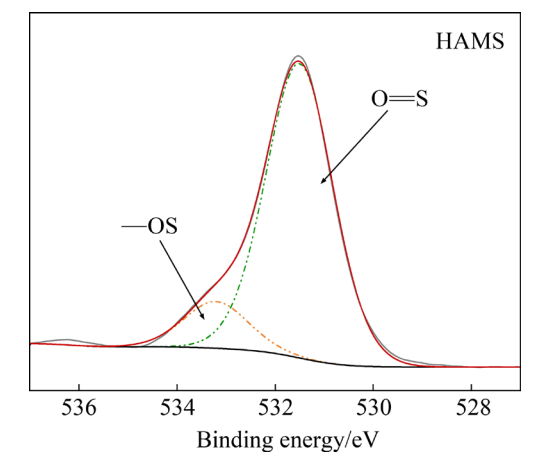


Fig. 7 Ols spectra of HAMS

on the surface of bare graphite (CuSO₄ treated graphite) [31–33]. Adsorption of HAMS on graphite shows a significant change in peak numbers compared to bare graphite. There were five peaks: 531.10 eV for surface hydroxyl (—OH), 531.56 eV for O=S, 532.31 eV for —COO-, 533.11 eV for —OS and 533.70 eV for H₂O [29–31,33]. In the graphite O 1s spectra of HAMS treatment, two additional peaks (531.56 and 533.11 eV) were generated, which just corresponded to the peak of the HAMS O 1s spectra. The peaks centered at 531.50 and 533.21 eV corresponded to O=S and —OS in the O 1s spectra of HAMS, respectively [29,30], confirming the adsorption of HAMS on graphite surfaces.

As displayed in Fig. 8(b) and Table 1, the O 1s spectra of sphalerite were fitted with three peaks. The peak at 530.09 eV was attributed to O in metal oxides [34]. The peak at 531.61 eV was attributed to hydroxyl bond (OH) [34]. The peak at 533.06 eV was assigned to organic oxygen, which was a result

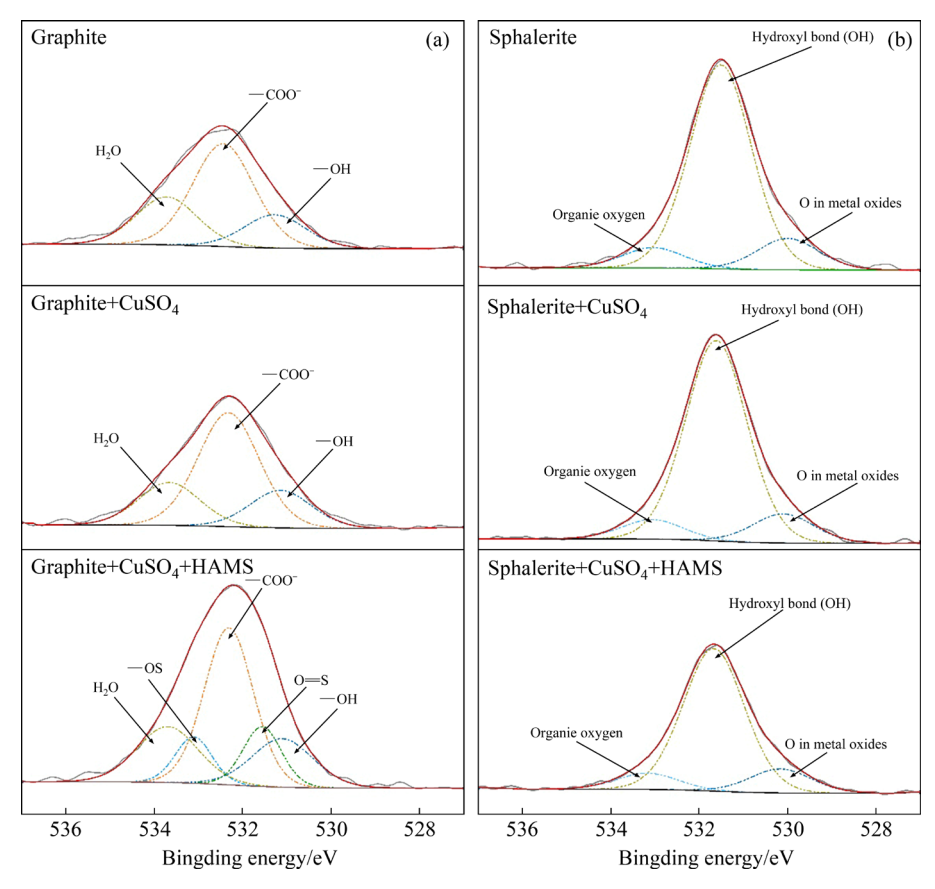


Fig. 8 O 1s spectra of graphite (a) and sphalerite (b) in the absence and in the presence of HAMS

Table 1 Fitting results of O 1s spectra for graphite and sphalerite

Sample	BE/eV	FWHM/eV	7 Assignment
HAMS	531.50	1.68	o=s
	533.21	1.60	-os
Bare graphite	531.28	1.70	—ОН
	532.45	1.70	—COO-
	533.73	1.70	H_2O
Graphite+ CuSO ₄	531.14	1.70	—OH
	532.32	1.70	—COO-
	533.67	1.70	H_2O
	531.10	1.70	—ОН
Graphite+	531.56	1.06	o=s
CuSO ₄ + HAMS	532.31	1.36	—COO_
	533.11	1.02	-os
	533.70	1.70	H ₂ O
Bare sphalerite	529.99	1.70	O in metal oxides
	531.51	1.70	Hydroxyl bond (OH)
	533.03	1.70	Organic oxygen
Sphalerite+ CuSO ₄	530.09	1.70	O in metal oxides
	531.61	1.70	Hydroxyl bond (OH)
	533.06	1.70	Organic oxygen
Sphalerite+	530.15	1.70	O in metal oxides
CuSO ₄ +	531.66	1.70	Hydroxyl bond (OH)
HAMS	533.16	1.70	Organic oxygen

BE: Binding energy; FWHM: Full width at half maximum

of carbon contamination [35]. There was no recognizable O 1s peak of HAMS on HAMS-treated sphalerite O 1s spectra, and its peaks were only slightly shifted compared to bare sphalerite. We were unable to determine if these minor alterations were caused by HAMS adsorption or the experimental environment. However, in comparison to graphite, HAMS exhibits no visible adsorption on sphalerite. The typical O 1s peaks of HAMS did not appear on HAMS-treated sphalerite.

3.4.2 S 2p

Considering the molecular structure of HAMS and the crystal structure of graphite, the S 2p spectra were analyzed. $2p_{1/2}$ and $2p_{3/2}$ doublets were fitted to the S 2p spectra. Their intensity ratio was 1:2, and their energy separation was 1.18 eV. The HAMS S 2p spectra are shown in Fig. 9. The peak fitting parameters and S 2p assignment are summarized in Table 2. The peak at 167.96 eV was assigned to $-SO_3^-$ [36].

Figure 10 presents the S 2p spectra of graphite and sphalerite in the absence and presence of HAMS. Table 2 summarizes the peak fitting parameters and the assignment of S 2p. As observed

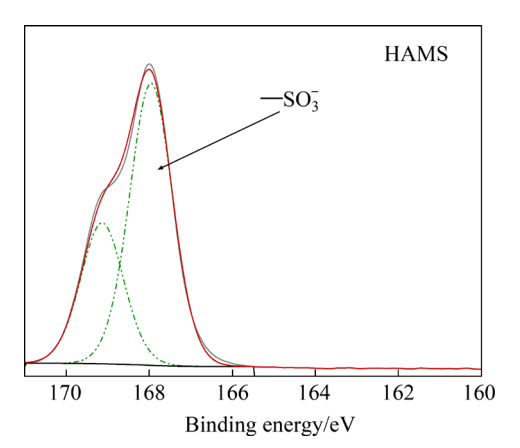


Fig. 9 S 2p spectra of HAMS

in Fig. 10(a) and Table 2, the peaks at 162.10 (162.00 eV) and 164.02 eV (164.05 eV) of bare graphite (CuSO₄ treated graphite) was assigned to the S 2p_{3/2} spectra of S²⁻ and polysulphide, respectively [37–40]. They could be caused by pyrite impurities in graphite and oxides on the pyrite surface [37,39], since pyrite is a prevalent mineral contaminant in natural flake graphite and

coal [41–44]. There was no obvious S 2p spectra peak of oxide on the surface of bare graphite (CuSO₄ treated graphite).

For graphite S 2p spectra after HAMS treatment, the peaks at 162.12 eV and 164.06 eV were assigned to S $2p_{3/2}$ spectra of S²⁻ and polysulphide, respectively [37–40]. The fitted S 2p spectra of sulfur oxides were split into two peaks at 168.08 and 169.26 eV. Obviously, the HAMS produced a peak in the S 2p spectra of sulfur oxides on graphite surfaces. The peaks of 168.08 and 169.26 eV were assigned to S $2p_{3/2}$ and S $2p_{1/2}$ of $-SO_3^-$ in HAMS.

As shown in Fig. 10(b) and Table 2, the peaks at 161.54 eV (161.54 eV) of bare sphalerite (CuSO₄ treated sphalerite) were assigned to S $2p_{3/2}$ of S²⁻ in ZnS and defect sulphide [35]. For sphalerite S 2p spectra after HAMS treatment, it was nearly identical to that of bare sphalerite, and there was no new peak. This result demonstrated that there was no visible adsorption of HAMS on the surface of sphalerite.

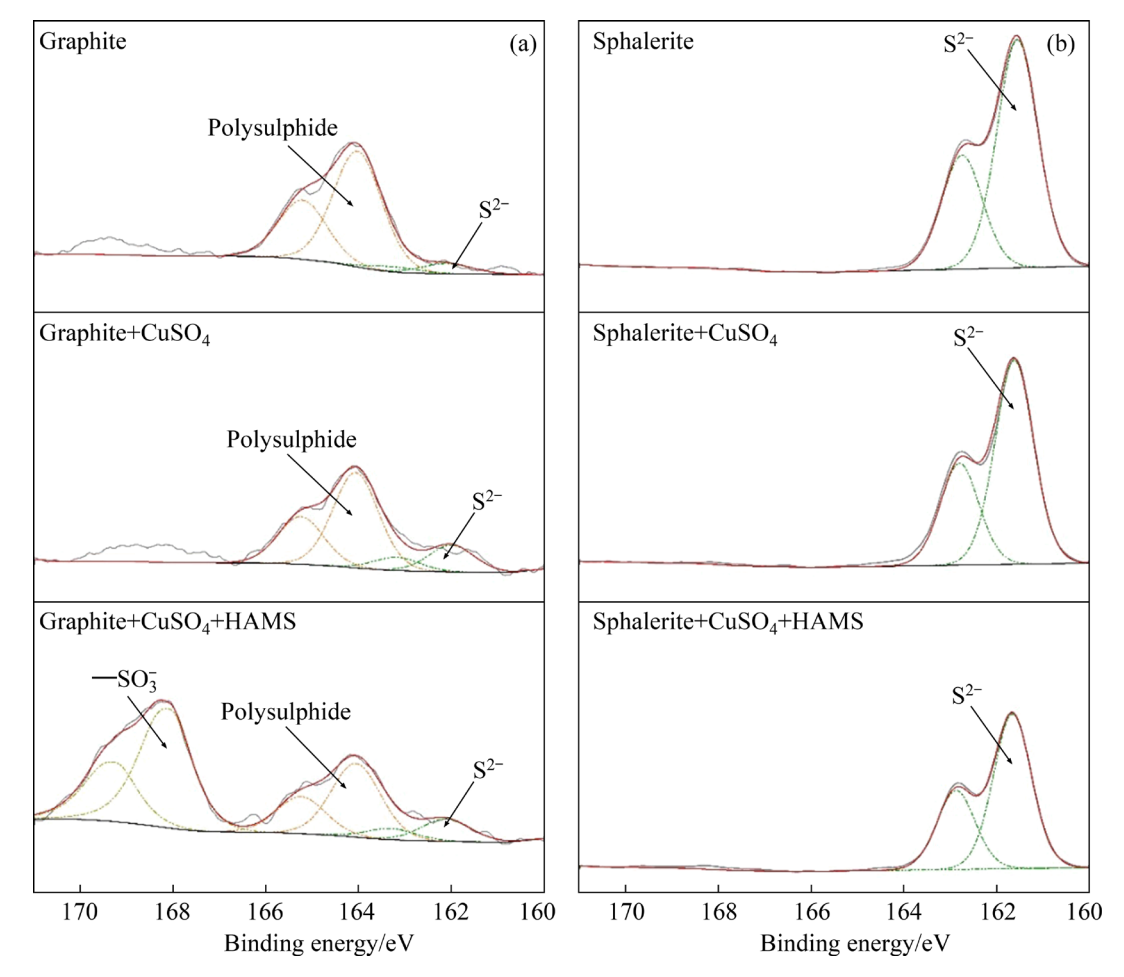


Fig. 10 S 2p spectra of graphite (a) and sphalerite (b) in the absence and in the presence of HAMS

Table 2 Fitting results of S 2p spectra for graphite and sphalerite

Sample	BE/eV	FWHM/eV	Assignment
HAMS	167.96	1.27	$-so_3^-$
Bare	162.10	1.30	S^{2-}
graphite	164.02	1.28	Polysulphide
Graphite+	162.00	1.30	S^{2-}
CuSO ₄	164.05	1.29	Polysulphide
Graphite+	162.12	1.30	S ²⁻
CuSO ₄ +	164.06	1.30	Polysulphide
HAMS	168.08	1.19	$-SO_3^-$
Bare	161.54	1.02	S ²⁻ (ZnS and
sphalerite	101.34		defect sulphide)
Sphalerite+	161.62	1.02	S ²⁻ (ZnS and
$CuSO_4$	101.02	1.02	defect sulphide)
Sphalerite+	161.66	1.01	S ²⁻ (ZnS and
CuSO ₄ +HAMS	101.00	1.01	defect sulphide)

3.5 Molecular dynamics simulation and possible separation mechanism

To further understand the depressing mechanism of HAMS, molecular dynamics simulation was used to explore the adsorption structure of HAMS on graphite surfaces in a water system. The initial structure is depicted in Fig. 11(a), and the equilibrium interfacial adsorption structure of HAMS on graphite surfaces is shown in Fig. 11(b). As displayed in Fig. 11(b), some HAMS molecules were laid on the graphite surface as a thin film, which prevented the exposure of the hydrophobic neutral graphite surface to water. Obviously, it was the most efficient adsorption mode of HAMS due to the largest proportion of graphite surface coverage. As displayed in Fig. 11(c), a water exclusion area exists between the graphite surface and the water reagent system. The hydrophobic naphthalene ring in HAMS was squeezed to the surface of graphite. Combining with the electric neutrality crystal structure of graphite, the hydrophobic force was more worthy of being considered the driving force of HAMS adsorption on the graphite surface [45]. As displayed in Fig. 11(d), many hydrogen bonds were formed between hydrophilic groups (-SO₃ and -OH) in HAMS and water molecules. It can be inferred that the formation of hydrogen bonds was the main reason for the hydrophilicity of the HAMS-treated graphite surface.

The results of molecular dynamics simulation demonstrated that the hydrophobic interaction between the naphthalene ring in HAMS and graphite ensures that HAMS can be stably adsorbed on the graphite surface, while the hydrogen bonds between hydrophilic groups in HAMS and water molecules ensure the hydrophilicity of HAMS-treated graphite surface.

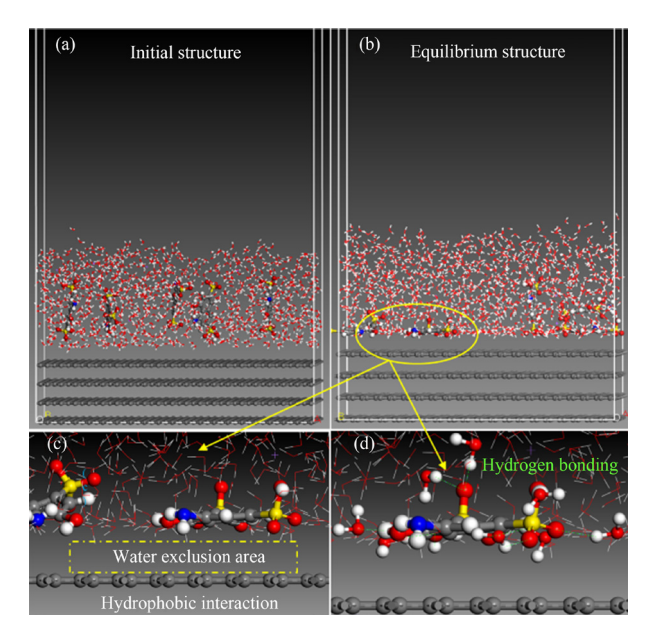


Fig. 11 Interfacial information of HAMS on graphite surfaces: (a) Initial structure; (b) Equilibrium structure; (c) Local detail of equilibrium structure; (d) Hydrogen bonding between HAMS and water in equilibrium structure

Based on all experimental results, we proposed a possible selective depressing mechanism of HAMS in the separation of graphite and sphalerite (Fig. 12). The Zeta potential test and XPS analysis demonstrated that HAMS was largely adsorbed on the graphite surface, while there was almost no adsorption of HAMS on the sphalerite surface. The FT-IR analysis and molecular dynamics simulation inferred that there was no strong chemical adsorption of HAMS on the graphite surface, and HAMS is mainly adsorbed on the graphite surface via its naphthalene ring by hydrophobic interaction.

4 Conclusions

(1) The micro-flotation of both single mineral flotation and mixed mineral flotation confirmed that HAMS could achieve selective separation of graphite and sphalerite. Under the optimum mixed

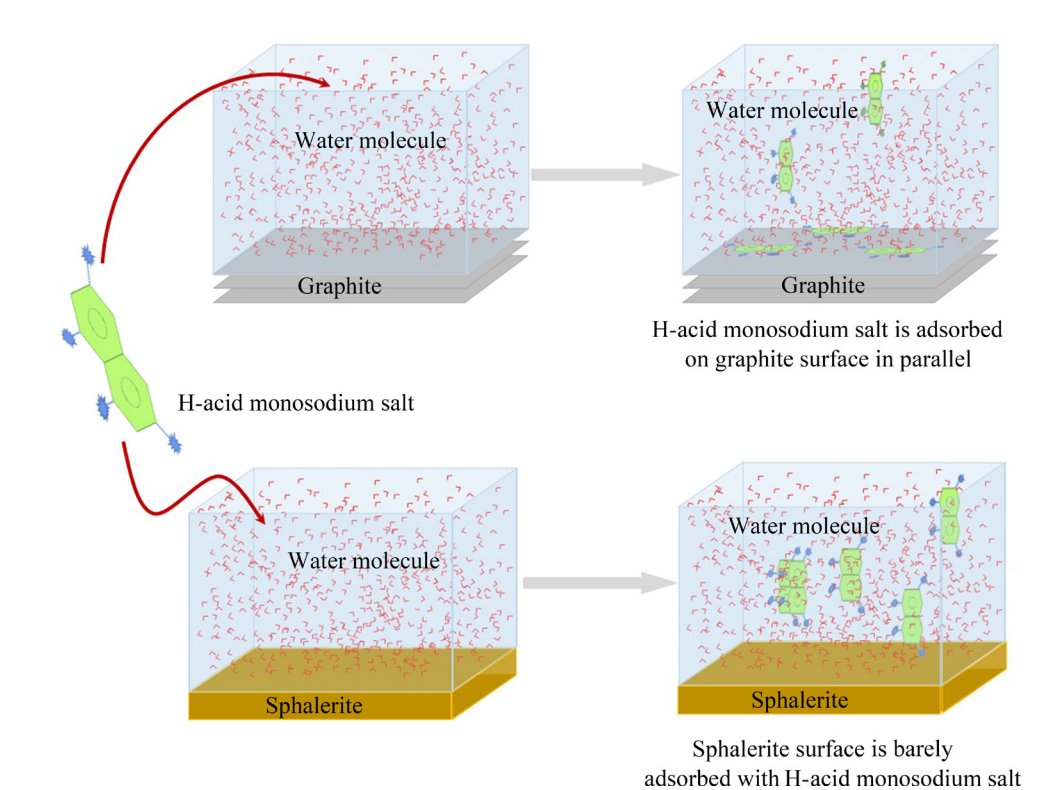


Fig. 12 Possible selective depressing mechanism of HAMS in separation of graphite and sphalerite

mineral flotation conditions, the recoveries of sphalerite and graphite in the flotation concentrate were 93.37% and 4.98%, respectively.

- (2) The Zeta potential tests indicated that HAMS was considerably adsorbed on the surface of graphite but virtually completely absent on the surface of sphalerite. XPS analysis further confirmed the difference in the adsorption of HAMS on the surfaces of graphite and sphalerite.
- (3) The FT-IR tests revealed that HAMS has no significant chemisorption on the surfaces of graphite and sphalerite. Based on molecular dynamics simulation analyses, hydrophobic interaction was observed between the naphthalene ring in HAMS and graphite, as well as hydrogen bonds between hydrophilic groups in HAMS and water molecules. They were inferred to be the driving force behind the adsorption and depression of HAMS on graphite.

Acknowledgments

This work was supported by the National Key R&D Program of China (Nos. 2022YFC2904501, 2019YFC1907803), the National Natural Science Foundation of China (No. 52004335), the Open Sharing Fund for Large-scale Instruments and Equipment of Central South University, China (No.

CSUZC202132), and the Key Laboratory of Hunan Province for Clean and Efficient Utilization of Strategic Calcium-containing Mineral Resources, China (No. 2018TP1002).

References

- [1] KAWASAKI K, SYMONS D T A, DAWBORN T. Paleomagnetism of the world-class century Zn-Pb-Ag deposits, Australia [J]. Journal of Geochemical Exploration, 2010, 106(1/2/3): 137–145.
- [2] SUGDEN T J, DEB M, WINDLEY B F. The tectonic setting of mineralisation in the Proterozoic Aravalli Delhi orogenic belt, NW India [J]. Developments in Precambrian Geology, 1990, 8: 367–390.
- [3] ZHU Xiao-qin, ZHANG Qian, HE Yu-liang, ZHU Cao-hui. The evolutions of lead and zinc in the rocks of the early earth's history ore-forming material source of the Proterozoic SEDEX type Pb–Zn deposits from the Langshan–Zhaertaishan district in Inner Mongolia, China [J]. Acta Mineralogica Sinica, 2005, 25(4): 325–333. (in Chinese)
- [4] JI Ya-na, SUN Ti-chang, JI Jun. The comparative study on two carbonaceous lead-zinc ores using pre-decarbonization [J]. China Mining Magazine, 2010, 146(2): 106–114. (in Chinese)
- [5] GUPTA N. Evaluation of graphite depressants in a polymetallic sulfide flotation circuit [J]. International Journal of Mining Science and Technology, 2017, 27(2): 285–292.
- [6] WANG Li-Cong, NI Xin-jiong, CAO Yu-Hua, CAO Guang-qun. Adsorption behavior of bisphenol A on CTAB-

- modified graphite [J]. Applied Surface Science, 2018, 428: 165-170.
- [7] CHIMONYO W, FLETCHER B, PENG Yong-jun. Starch chemical modification for selective flotation of copper sulphide minerals from carbonaceous material: A critical review [J]. Minerals Engineering, 2020, 156: 106522.
- [8] CHIMONYO W, FLETCHER B, PENG Yong-jun. The differential depression of an oxidized starch on the flotation of chalcopyrite and graphite [J]. Minerals Engineering, 2020, 146: 106114.
- [9] BEAUSSART A, MIERCZYNSKA-VASILEV A M, HARMER S L, BEATTIE D A. The role of mineral surface chemistry in modified dextrin adsorption [J]. Journal of Colloid and Interface Science, 2011, 357(2): 510–520.
- [10] BOOTH R B. Depression of gangue during flotation [P]. US-2211686-A , 1940-08-13.
- [11] PUGH R J. Macromolecular organic depressants in sulphide flotation—A review, 1. Principles, types and applications [J]. International Journal of Mineral Processing, 1989, 25(1/2): 101–130.
- [12] RAJU G B, HOLMGREN A, FORSLING W. Adsorption of dextrin at mineral/water interface [J]. Journal of Colloid and Interface Science, 1997, 193(2): 215–222.
- [13] SOLARIS J A, de ARAUJO A C, LASKOWSKI J S. The effect of carboxymethyl cellulose on the flotation and surface properties of graphite [J]. Coal Preparation, 1986, 3(1): 15–31.
- [14] SOLONGO S K, GOMEZ-FLORES A, ILYAS S, KIM H. Roles of solution chemistry and reagent–reagent interaction on carboxymethylcellulose adsorption onto graphite and implications on its floatability [J]. Minerals Engineering, 2021, 167(1): 106873.
- [15] LIU Qi, LASKOWSKI J S. The role of metal hydroxides at mineral surfaces in dextrin adsorption, I. Studies on modified quartz samples [J]. International Journal of Mineral Processing, 1989, 26(3/4): 297–316.
- [16] LIU Qi, LASKOWSKI J S. The role of metal hydroxides at mineral surfaces in dextrin adsorption, II. Chalcopyritegalena separations in the presence of dextrin [J]. International Journal of Mineral Processing, 1989, 27(1/2): 147–155.
- [17] LIU Qi, LASKOWSKI J S. The interactions between dextrin and metal hydroxides in aqueous solutions [J]. Journal of Colloid and Interface Science, 1989, 130(1): 101–111.
- [18] RASHCHI F, FINCH J A, SUI C. Action of DETA, dextrin and carbonate on lead-contaminated sphalerite [J]. Colloids and Surfaces A: Physicochemical and Engineering Aspects, 2004, 245(1/2/3): 21–27.
- [19] SUBRAMANIAN S, LASKOWSKI J S. Adsorption of dextrin onto graphite [J]. Langmuir, 1993, 9(5): 1330–1333.
- [20] DU Hao, MILLER J D. Adsorption states of amphipatic solutes at the surface of naturally hydrophobic minerals: A molecular dynamics simulation study [J]. Langmuir 2007, 23(23): 11587–11596.
- [21] ZHANG Zi-wei, WANG Fang, YANG Wei-ben, YANG Zhen, LI Ai-min. A comparative study on the adsorption of 8-amino-1-naphthol-3, 6-disulfonic acid by a macroporous amination resin [J]. Chemical Engineering Journal, 2016, 283: 1522–1533.

- [22] SWAMINATHAN K, PACHHADE K, SANDHYA S. Decomposition of a dye intermediate, (H-acid) 1 amino-8-naphthol-3,6 disulfonic acid in aqueous solution by ozonation [J]. Desalination, 2005, 186(1/2/3): 155–164.
- [23] VUČINIĆ D R, LAZIĆ P M, ROSIĆ A A. Ethyl xanthate adsorption and adsorption kinetics on lead-modified galena and sphalerite under flotation conditions [J]. Colloids and Surfaces A: Physicochemical and Engineering Aspects, 2006, 279(1/2/3): 96–104.
- [24] WEI Qian, DONG Liu-yang, JIAO Fen, QIN Wen-qing, PAN Zu-chao, CUI Yan-fang. The synergistic depression of lime and sodium humate on the flotation separation of sphalerite from pyrite [J]. Minerals Engineering, 2021, 163: 106779
- [25] GAN Yong-gang, DENG Rong-dong, LIU Quan-jun. Surface characteristics, collector adsorption, and flotation response of covellite in oxidizing environment [J]. Transactions of Nonferrous Metals Society of China, 2022, 32(2): 657–667.
- [26] QIU Ting-sheng, LI Guo-dong, LI Xiao-bo, YAN Hua-shan, LIU Chen. Influence of high concentration Zn²⁺ on floatability of sphalerite in acidic system [J]. Transactions of Nonferrous Metals Society of China, 2021, 31(7): 2128–2138.
- [27] WANG Zhou-jie, XU Long-hua, WU Hou-qin, ZHOU Huan, MENG Jin-ping, HUO Xiao-mei, HUANG Ling-yun. Adsorption of octanohydroxamic acid at fluorite surface in presence of calcite species [J]. Transactions of Nonferrous Metals Society of China, 2021, 31(12): 3891–3904.
- [28] ZHONG Chun-hui, FENG Bo, CHEN Yuan-gan, GUO Meng-chi, WANG Hui-hui. Flotation separation of molybdenite and talc using tragacanth gum as depressant and potassium butyl xanthate as collector [J]. Transactions of Nonferrous Metals Society of China, 2021, 31(12): 3879–3890.
- [29] RUANGCHUAY L, SCHWANK J, SIRIVAT A. Surface degradation of α-naphthalene sulfonate-doped polypyrrole during XPS characterization [J]. Applied Surface Science, 2002, 199(1/2/3/4): 128–137.
- [30] SHUTTHANANDAN V, NANDASIRI M, ZHENG Jian-ming, ENGELHARD M H, XU Wu, THEVUTHASAN S, MURUGESAN V. Applications of XPS in the characterization of Battery materials [J]. Journal of Electron Spectroscopy and Related Phenomena, 2019, 231: 2–10.
- [31] FERRAH D H, HAMANDA R, GALHENAGE R P, BRUCE J P, BABORE A D, HUNT A, WALUYO I, HEMMINGER J C. Wet chemical growth and thermocatalytic activity of Cu-based nanoparticles supported on TiO₂ nanoparticles/HOPG: In situ ambient pressure XPS study of the CO₂ hydrogenation reaction [J]. ACS Catalysis, 2019, 9(8): 6783-6802.
- [32] EBITANI K, KONNO H, TANAKA T, HATTORI H. In-situ XPS study of zirconium oxide promoted by platinum and sulfate ion [J]. Journal of Catalysis, 1992, 135(1): 60–67.
- [33] YU Lin-ling, CAO Wen, WU Shi-chuan, YANG Cao, CHENG Jian-hu. Removal of tetracycline from aqueous solution by MOF/graphite oxide pellets: Preparation, characteristic, adsorption performance and mechanism [J]. Ecotoxicology and Environmental Safety, 2018, 164: 289–296.

- [34] LAI Hao, DENG Jiu-shuai, WEN Shu-ming, LIU Quan-jun. Elucidation of lead ions adsorption mechanism on marmatite surface by PCA-assisted ToF-SIMS, XPS and zeta potential [J]. Minerals Engineering, 2019, 144: 106035.
- [35] LIU Jian, EJTEMAEI M, V NGUYEN A, WEN Shu-ming, ZENG Yong. Surface chemistry of Pb-activated sphalerite [J]. Minerals Engineering, 2020, 145: 106058.
- [36] NASEF M M, SAIDI H. Surface studies of radiation grafted sulfonic acid membranes: XPS and SEM analysis [J]. Applied Surface Science, 2006, 252(8): 3073–3084.
- [37] LI De-jian, LIU Chen-rui, LIU Yun, CHEN Xue-min, WU Wei-feng, LI Feng, TIAN Jiang, DANG Zhi. Tannic acid as an eco-friendly natural passivator for the inhibition of pyrite oxidation to prevent acid mine drainage at the source [J]. Applied Surface Science, 2022, 591: 153172.
- [38] LAAJALEHTO K, KARTIO I, SUONINEN E. XPS and SR-XPS techniques applied to sulphide mineral surfaces [J]. International Journal of Mineral Processing, 1997, 51(1/2/3/4): 163–170.
- [39] XIAN Yong-jun, WANG Yi-jie, WEN Shu-ming, NIE Qi, DENG Jiu-shuai. Floatability and oxidation of pyrite with different spatial symmetry [J]. Minerals Engineering, 2015, 72: 94–100.
- [40] ZHANG Yan, CHEN Zhen, ZI Fu-ting, HU Xian-zhi, YANG Peng, CHENG Hui-ling, CHEN Yun-long, QIN Xue-cong, CHEN Shu-liang, HE Pu-qiang, LIN Yue, ZHAO Li. New

- insights into the oxidation mechanism of pyrite in copper-containing sulfuric acid: An electrochemical, AFM, Raman spectroscopy and XPS investigation [J]. Journal of the Electrochemical Society, 2021, 168(6): 061502.
- [41] DENG Jun, MA Xiao-feng, ZHANG Yu-tao, LI Ya-qing, ZHU Wen-wen. Effects of pyrite on the spontaneous combustion of coal [J]. International Journal of Coal Science and Technology, 2015, 2(4): 306–311.
- [42] LIU Hai-ying, LAO De-ping, LI Chong-de, SHEN Shi-fu. Floatation technical study of Luobei flake graphite in Heilongjiang province [J]. China Mining Magazine, 2015, 24(S2): 182–185. (in Chinese)
- [43] OUYANG Zhi-jun. An experimental research on recycling graphite and vanadium comprehensively from graphite ore in Jiangxi [M]. Wuhan: Wuhan University of Technology, 2016. (in Chinese)
- [44] ZHANG Lin-yan, QIU Yang-shuai, HUANG Wen, YANG Hui-qun. Experimental research on beneficiation of graphite ore from Anshan area [J]. Non-Metallic Mines, 2011, 34(5): 21–23. (in Chinese)
- [45] XIA Yang-chao, XING Yao-wen, LI Ming, LIU Min, TAN Jin-liong, CAO Yi-jun, GUI Xia-hui. Studying interactions between undecane and graphite surfaces by chemical force microscopy and molecular dynamics simulations [J]. Fuel, 2020, 269: 117367.

H 酸单钠盐在石墨与闪锌矿浮选分离中的选择性抑制机理

曾 勇 ^{1,2}, 王 翠 ^{1,2}, 何剑锋 ^{1,2}, 华中宝 ^{1,2}, 程 恺 ^{1,2}, 伍喜庆 ^{1,2}, 孙 伟 ^{1,2}, 王 丽 ^{1,2}, 胡家城 ³, 唐鸿鹄 ^{1,2}

- 1. 中南大学 资源加工与生物工程学院,长沙 410083;
- 2. 中南大学 战略含钙矿物资源清洁高效利用湖南省重点实验室,长沙 410083;
 - 3. 中国科学院 过程工程研究所 多相复杂系统国家重点实验室, 北京 100190

摘 要:采用纯矿物浮选实验、傅里叶变换红外光谱(FT-IR)测试、Zeta 电位测试、X 射线光电子能谱(XPS)分析和分子动力学模拟研究 H 酸单钠盐(HAMS)存在下石墨和闪锌矿的浮选行为和分离、抑制机理。在最佳浮选条件下,混合浮选精矿中闪锌矿和石墨的回收率分别为 93.37%和 4.98%。Zeta 电位测试和 XPS 分析表明,HAMS 大量吸附在石墨表面,而在闪锌矿表面几乎不吸附。FT-IR 测试表明,HAMS 在石墨表面没有明显的化学吸附。分子动力学模拟结果表明,HAMS 中的萘环与石墨之间的疏水相互作用是导致 HAMS 吸附在石墨表面的主要原因。关键词:H 酸单钠盐;石墨;闪锌矿;浮选分离;分子动力学模拟

(Edited by Xiang-qun LI)